IOP Publishing Measurement Science and Technology
Meas. Sci. Technol. **31** (2020) 035107 (11pp) https://doi.org/10.1088/1361-6501/ab55f9

# A novel dynamic calibration method using polyvinylidene fluoride piezoelectric film for ultrasonic vibration sensing application

**Le Song[1], Yujin Wang[1], Yifan Jia[1], Clarence Augustine T H Tee[2,3], Hu Gong[1] and Yelong Zheng[1]**

[1] State Key Laboratory of Precision Measuring Technology and Instruments, Tianjin University, Tianjin 300072, People's Republic of China
[2] Faculty of Engineering, Department of Electrical Engineering, University of Malaya, Kuala Lumpur 50603, Malaysia
[3] Faculty of Engineering, Centre of Advanced Research Enabler Facility, University of Malaya, Kuala Lumpur 50603, Malaysia

E-mail: zhengyelongby@163.com

Received 25 April 2019, revised 27 October 2019
Accepted for publication 11 November 2019
Published 27 December 2019

**Abstract**

Ultrasound has a wide range of applications in many fields. It has great significance in measuring the ultrasonic signal generated in process applications, such as ultrasonic vibration cutting and ultrasonic testing. However, its high frequency characteristics make it difficult to measure the ultrasonic signal. A novel sensor is proposed herewith, exhibiting excellent qualities such as good flexibility and quick response using polyvinylidene fluoride (PVDF), suitable for measuring ultrasonic frequency bands. The piezoelectric constant is a vital factor, influencing the accuracy of the measurement. The frequency of existing calibration methods for the piezoelectric constant is below 1 kHz. At present, as per our literature reviews, there is no existing or suitable method for calibrating PVDF under ultrasonic frequency. In this paper, a novel calibration method of the piezoelectric constant based on the 'falling ball' is presented, which could calibrate the constant dynamically at about 2.5 kHz. A steel ball is released from a static state, then it falls onto a thin rod placed on a dynamometer. By loading the mass of the steel ball with different masses at the falling height, different frequencies of the vertical dynamic impact can be produced. The calibration result of $d_{33}$ is 20.80 pC $N^{-1}$ with a relative uncertainty of 1.28%, and the responsivity $K$ is 1.600 pC/$\mu\varepsilon$ with a relative uncertainty of 1.896%. Finally, taking an ultrasonic transducer and horn as an example, the strain produced by the horn is measured with the calibrated PVDF film at ultrasonic frequency. It is proven that the piezoelectric constant calibrated by this method is suitable for ultrasonic frequency measurement.

Keywords:polyvinylidene fluoride, falling ball method, calibration of the piezoelectric constant, ultrasonic frequency

(Some figures may appear in colour only in the online journal)

## 1. Introduction

Recently, with the development of ultrasound technology, humans' production and lifestyle have greatly improved in various areas. In the medical field, for example, ultrasound can be used to disintegrate kidney stones in the human body [1]. In the industrial field, Verhaagen *et al* [2] used ultrasound to design a 'cleaning challenge device' and Feng *et al* [3] studied the process of the ultrasonic humidifier. In the field of measurement, Zhou *et al* [4] used ultrasonic tests to evaluate the laser weld width. Furthermore, in the field of machining, Chu *et al* [5, 6] proved that ultrasonic assisted drilling could reduce the friction, temperature and torque, leading to elongation of tool life. During the ultrasonic machining process,

 

the measurement of the cutting force is the focus of research. Totis *et al* [7] designed an innovative dynamometer for triaxial cutting force measurement in turning [7] and Kim *et al* [8] measured the milling force with a piezoelectric force platform. Evidently, there is a wide application of ultrasonic waves in areas of production and in our daily life. Due to the high-frequency component of ultrasonic waves, measuring the signals in the ultrasonic frequency band requires sensors with quick response and large bandwidth.

As a new type of polymer sensor, polyvinylidene fluoride (PVDF) piezoelectric film has excellent piezoelectric performance. Specifically, it is characterized by its light weight, good flexibility, wide frequency response range, high responsivity and easy installation [9]. However, there are also some disadvantages, such as the high internal resistance of the sensor, low output capability and poor low-frequency sensing characteristics, and it can only meet linear requirements within a certain range. In addition, it is easily affected by external environmental factors such as the temperature [10]. Bae *et al* made an ultra-thin sensor with PVDF and ZnO which focused on improving the responsivity and which could detect pressure changes of about 10 Pa [11]. Persano prepared a high-performance pressure sensor that could perceive a tiny pressure of about 0.1 Pa [12]. Hu *et al* made a wrist sensor with PVDF. To measure the responsivity of the sensor quantitatively, the experiment measured the force by using the resistance strain gauge (FRS402) and found that when the excitation signal exceeded 15 Hz, the responsivity of the sensor was always stable at 3.10 pC $N^{-1}$ [13]. Thus, the responsivity of PVDF film is an important factor in the accuracy of measurement results. PVDF can sense the signal by pasting on the surface of the workpiece to be measured. This method has less influence on the original system, and has better dynamic response and higher responsivity. It is an ideal choice for measurement at ultrasonic frequency [14]. AlMohimeed *et al* investigated an improvement of the ultrasonic performance of a wearable ultrasonic sensor using double-layer PVDF films [15].

However, the accuracy of the measurement results largely depends on the piezoelectric constant of the PVDF. Common methods for calibrating the piezoelectric constant include the dropping hammer method, equal-strength beam method, the Berlincourt system and the Hopkinson bar technique. The dropping hammer method uses a hammer which is dropped from a certain height on a piston. The piston interacts with silicone oil to create a dynamic force and the piezoelectric constant is calibrated by a standard pressure sensor. It showed that the PVDF film has high linearity and good repeatability, but the time of the impact force was a little longer [16]. The principle of the equal-strength beam method is that the strain on the beam is equal everywhere when it is excited by the signal generator. The PVDF film and the standard strain gauge are attached to the equal-strength beam. The calibration frequency of this method is generally below 100 Hz [17]. In the Berlincourt system, the quantities measured are force and charge. The traceable calibration of the charge is relatively straightforward, but the calibration of force is more difficult [18]. It is a quasi-static calibration method and cannot represent the piezoelectric constant at higher frequency. The modified Mach–Zehnder interferometer and optical Doppler vibrometer can accurately measure small deformation of the film under the action of an electric field [19]. As for the Hopkinson bar technique, a bullet hits the input bar at a high speed and generates a stress wave. The PVDF film and strain gauge are placed between the input bar, a workpiece and the output bar. The stress on both end faces of the workpiece will be balanced. That is to say, the piezoelectric film and the strain gauge are subjected to the same stress. Van Nuffel *et al* used the Hopkinson bar method to calibrate the responsivity of the piezoelectric sensor with an uncertainty of 1.28% [20]. Although the dynamic performance of this method is relatively good, it is mainly used to calibrate the piezoelectric constant in the direction perpendicular to the surface of the PVDF film (thickness direction) and cannot calibrate the piezoelectric constant in the direction parallel to the film (tensile direction). In this paper, we will focus on this problem. Firstly, a new simple calibration method based on the falling ball system is proposed. This system can calibrate the piezoelectric constant in both the thickness and tensile direction of the PVDF film dynamically as well as at ultrasonic frequencies. Then taking the horn in the ultrasonic assisted vibration cutting system as an example, we use the PVDF film calibrated by the falling ball method to measure the strain generated on the horn. Finally, this experiment can lay a certain theoretical and experimental basis for the subsequent measurement and application of PVDF film in other ultrasonic fields.

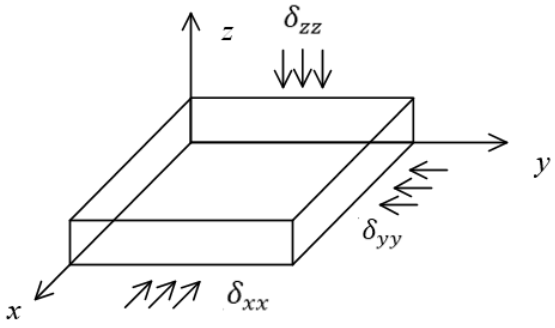


**Figure 1.** Schematic of PVDF film.

## 2. Experimental principle

### 2.1. Operating principle of PVDF film

As shown in figure 1, when PVDF film is deformed mechanically by a force, it will generate opposite charges on both sides of the film [21]. The output charge of PVDF film is as below:

$$Q = (d_{31}\delta_{xx} + d_{32}\delta_{yy} + d_{33}\delta_{zz})S, \tag{1}$$

where $Q$ is the output charge; $d_{31}$, $d_{32}$ and $d_{33}$ are the piezoelectric constants which are related to the charge generated on the $z$-plane to the stress in the $x$, $y$ and $z$ direction; $\delta_{xx}$, $\delta_{yy}$ and $\delta_{zz}$ are the stress in the $x$, $y$ and $z$ direction; and $S$ is the area of the PVDF film.

According to the direction of the force applied to the PVDF film, it can be divided into two working modes. One

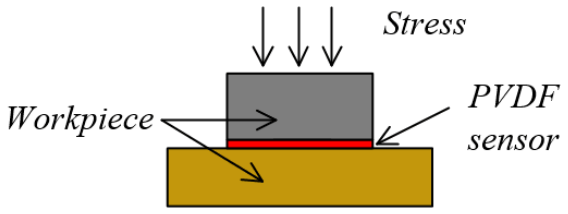


**Figure 2.** Diagram of thickness mode.

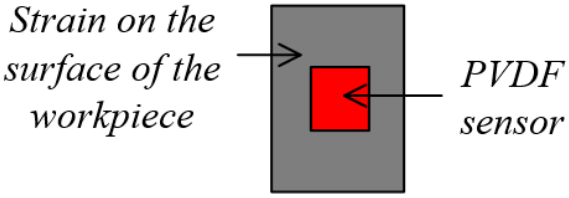


**Figure 3.** Diagram of tensile mode.

is thickness mode and the other is tensile mode. In these two modes, equation (1) can be further simplified separately.

### 2.2. Modes of PVDF film

*2.2.1. Thickness mode.* As shown in figure 2, when the PVDF film operates in thickness mode, it is generally considered that the PVDF film is stuck on the rigid material. The stress in the $x$ and $y$ directions is zero. Only the stress in the $z$ direction changes the thickness of the PVDF film. At this time, equation (1) can be written as:

$$Q = d_{33}\delta_{zz}S. \tag{2}$$

*2.2.2. Tensile mode.* When the PVDF film operates in the tensile mode, it is generally considered that the surface of the material to which the PVDF film is attached generates a strain. The stress in the $z$ direction is zero. As shown in figure 3, the output charge can be regarded as the result of the strain in each direction acting in the polarization direction of the film. Equation (1) can be written as [22]:

$$Q = (d_{31}\varepsilon_1 + d_{32}\varepsilon_2)E_{\mathrm{PVDF}}S, \tag{3}$$

where $d_{31}$ and $d_{32}$ are piezoelectric constants which relate to the charge generated on the $z$-plane to the stress in the $x$ and $y$ direction, $E_{\mathrm{PVDF}}$ is the Young's modulus of the PVDF, and $\varepsilon_1$ and $\varepsilon_2$ are the strain of the structure where PVDF is pasted. If the strain is generated only in the $x$ direction or $y$ direction, equation (3) can be simplified to:

$$Q = d_{31}E_{\mathrm{PVDF}}\varepsilon S \text{ or } Q = d_{32}E_{\mathrm{PVDF}}\varepsilon S. \tag{4}$$

### 2.3. Uniform strain generation

It is not easy to generate a traceable and measurable sinusoidal force of high frequency, so we used the impact force to calibrate $d_{31}$ and $d_{32}$. In the process of ultrasonic assisted machining, there are many impact phenomena. The constant of PVDF used for ultrasonic machining will be more accurate if calibrated by impact.

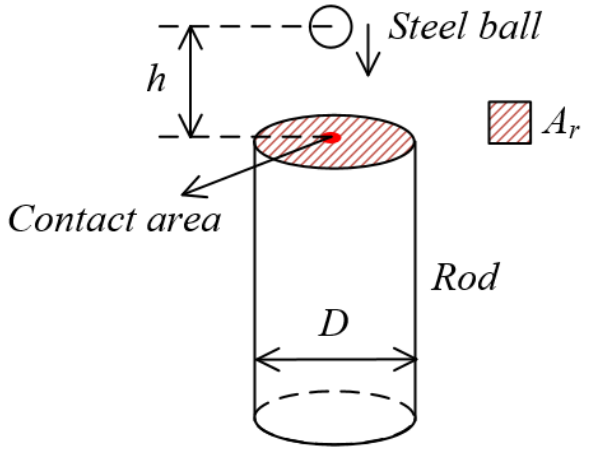


**Figure 4.** The position relationship between the ball and the rod.

An impact force can be generated by a steel ball in freefall hitting the surface. As shown in figure 4, the ball hits a vertical rod. The contact area during the impact between the ball and the rod is the contact between the sphere and the plane. So the impact of the ball can be thought of as a point load. In the same cross-section, the closer to the position of the impact, the greater strain of the rod will be produced. That is to say, the impact force will generate non-uniform stress in the same cross-section of the rod. However, according to Saint Venant's principle, assuming that the diameter of a cylindrical rod is $D$ and its length is $l_0$, the height of the non-uniform region is approximately 1 to 2 times $l_0$. If $l_0 \gg D$, even if the force applied to the end surface of the rod is not uniform, when the axial distance is more than 2D, the stress on the cross-section can be regarded as uniform. It is generally considered that on the rod mentioned above, as long as it meets the condition $l_0 > 10\mathrm{D}$, the wave generated by an impact is a 1D longitudinal wave. Thus, the stress generated in the uniform position is:

$$\delta_{zz} = \frac{F}{A_{\mathrm{r}}} = \frac{4F}{\pi D^2}, \tag{5}$$

where $F$ is the non-uniform axial impact and $A_{\mathrm{r}}$ is the cross-sectional area of the rod.

If the length of the rod is set as 1.2 m and the diameter as 0.024 m, according to the simulation software as shown in figure 5, the stress tends to be the same under the position of 0.04 m from the upper end of the rod.

## 3. Experimental scheme

### 3.1. Calibrating $d_{33}$ in thickness mode

As shown in figure 6, a dynamometer is placed horizontally in the buffer box, and a thin rod is placed vertically on the dynamometer. The falling ball machine can attract the ball and release it from rest, which will generate an impact. Then we adjust the position of the rod in order to make the impact position as close as possible to the central axis of the rod. The PVDF film is placed between the rod and the dynamometer. When the falling ball hits the bar, the PVDF film will be under

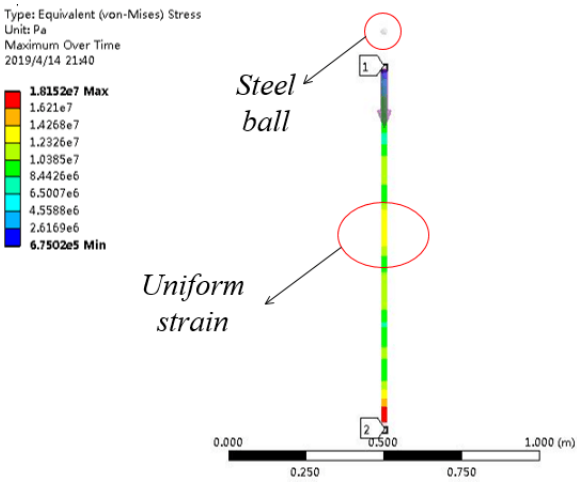


**Figure 5.** Simulation of the ball and the rod.

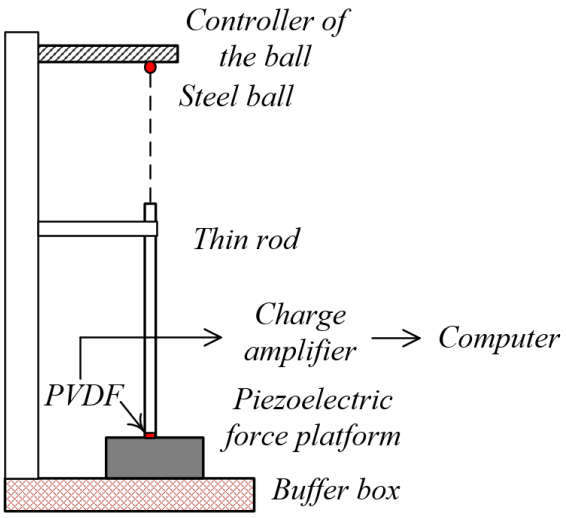


**Figure 6.** Calibration diagram of piezoelectric constant $d_{33}$.

a uniform vertical pressure and generate charge. The output of the PVDF film is amplified by a charge amplifier and transmitted to the computer by a data acquisition card. According to the voltage displayed on the computer, the output charge $Q$ of the PVDF can be found. The force $F$ on the PVDF film can be measured by the dynamometer. According to equation (2), taking the dynamometer as the measurement datum, the piezoelectric constant $d_{33}$ of the PVDF film can be calibrated by:

$$d_{33} = F/Q. \tag{6}$$

### 3.2. Calibrating $d_{31}$ in tensile mode

As shown in figure 7, the calibration method of $d_{31}$ is similar to 3.1. The steel ball falls from the falling machine and hits the rod. The vertical force measured by the dynamometer is $Fz$ and the strain produced by the rod in the vertical direction is:

$$\varepsilon = \delta_{zz}/Z = 4Fz/E\pi D^2, \tag{7}$$

where $E$ is the Young's modulus of the rod. The PVDF film is pasted on the middle part of the rod with double-sided tape. At

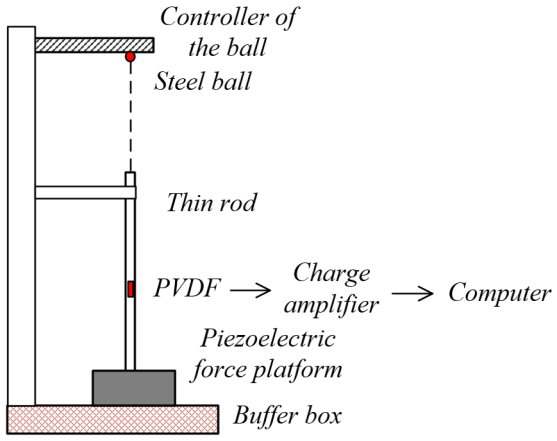


**Figure 7.** Calibration diagram of responsivity $K$.

this time, equation (4) is used to represent the output charge of the PVDF film. The strain responsivity of the PVDF film is defined as the ratio of the change in charge $\Delta Q$ to the change in strain $\Delta\varepsilon$, and the expression is [23]:

$$K = \Delta Q/\Delta\varepsilon. \tag{8}$$

## 4. Experiments and analysis

### 4.1. Equipment

*4.1.1. PVDF and thin rod.* The output charge of PVDF represents the average stress on the area it is pasted. In order to reflect the strain of a small area better, a smaller PVDF has been chosen which is a 5 mm diameter circular patch. The thin rod should meet the condition of $l_0 > 10D$. Here we select $GCr_{15}$ as the material of the rod. The specific parameters of the thin rod are shown in table 1.

*4.1.2. Dynamometer and charge amplifier.* The YDC-III-09 piezoelectric force measuring platform and YE5850B charge amplifier are selected as the dynamometer to measure three forces in the orthogonal direction. The dynamometer is the measurement datum of the calibration process, and has a certificate of verification. The data issued by it can be traced to the national standards of measurement. The results of the calibration are shown in table 2.

Under this charge responsivity and 1000 times of the charge amplifier, the relationship between the force value and the output voltage is 1:1; that is, the voltage of 1 mV represents a force of 1 N. Meanwhile, the tiny charge produced by the PVDF film also needs to be amplified by the charge amplifier. The amount of charge $Q$ = output voltage (mV)/amplification times (mV/pC). There are four amplification options: 1, 10, 100 and 1000.

*4.1.3. The falling ball machine.* The falling ball machine is an instrument that can control the steel ball to be released from static state. There is an electromagnet chuck controlled by a circuit, which can generate electromagnetic force to attract the steel ball. After pressing the falling key, the power supply will be cut off and the magnetic force will disappear. Then the steel

**Table 1.** Parameters of the rod.

| Length | Diameter | Young's modulus | Poisson's ratio |
|---|---|---|---|
| 1.2 m | 16 mm | 208 GPa | 0.3 |

**Table 2.** Calibration results of dynamometer.

| Indicator | $F_x$ | $F_y$ | $F_z$ |
|---|---|---|---|
| Measuring range (N) | 1000 | 1000 | 2000 |
| Charge responsivity (pC $N^{-1}$) | 8.92 | 8.50 | 3.75 |
| The linear error (%) | 0.08 | 0.08 | 0.19 |
| Repeatability error (%) | 0.17 | 0.08 | 0.19 |

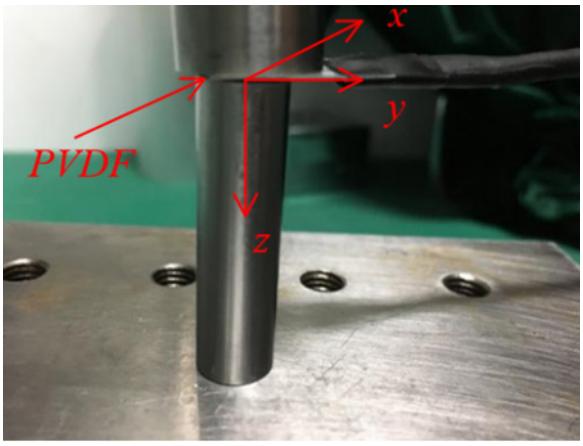


**Figure 8.** Experimental diagram of calibrating $d_{33}$.

ball will drop from static state. The weights of the available steel ball are 55 g, 64 g, 110 g, 225 g and 535 g. The drop height ranges from 0 to 2000 mm, which can be read from the scale on the drop club. The precision of the scale is 1 mm. According to the kinetic energy theorem, by increasing the mass of the steel ball and the falling height, the impact will be larger. Limited by the range of the dynamometer and charge amplifier, a steel ball of 55 g has been chosen for the experiments.

### *4.2. Calibration of piezoelectric constant in thickness mode*

The PVDF can only detect the varying forces and deformations, so the PVDF will not produce charge when the rod is statically pressed on the PVDF. The influence of the gravity of the rod can be ignored. In order to prevent damage on the PVDF film being caused by horizontal movement of the rod during the experiment, a small metal cylinder was placed between the rod and the dynamometer. As shown in figure 8, the PVDF film was fixed between the small cylinder and the rod with double-sided tape, to ensure that the PVDF film was under uniform stress.

The mass of the steel ball used in the experiment was 55 g and the falling heights ranged from 1.5 cm to 0.5 cm. The amplification time of the charge was 1 and the dynamometer was 10. The measurement results are shown in figure 9(a). There is more than one impact during each fall, and one of

**Table 3.** Calibration data of $d_{33}$.

| $h$ (cm) | $F_z$ (N) | $Q$ (pC) | $h$ (cm) | $F_z$ (N) | $Q$ (pC) |
|---|---|---|---|---|---|
| 0.5 | 40.5 | 874.3 | 1.0 | 117.39 | 2543 |
| 0.5 | 39.58 | 888.4 | 1.1 | 126.3 | 2566 |
| 0.5 | 41.75 | 903 | 1.1 | 130.1 | 2775 |
| 0.6 | 53.31 | 1136 | 1.1 | 127.9 | 2707 |
| 0.6 | 53.53 | 1139 | 1.3 | 149.8 | 3139 |
| 0.6 | 52.34 | 1108 | 1.3 | 154.5 | 3192 |
| 0.8 | 82.61 | 1709 | 1.3 | 164.3 | 3304 |
| 0.8 | 82.61 | 1786 | 1.5 | 200.1 | 4114 |
| 0.8 | 83.92 | 1855 | 1.5 | 198.4 | 4074 |
| 1.0 | 112.7 | 2327 | 1.5 | 201.5 | 4134 |
| 1.0 | 115.5 | 2477 | | | |

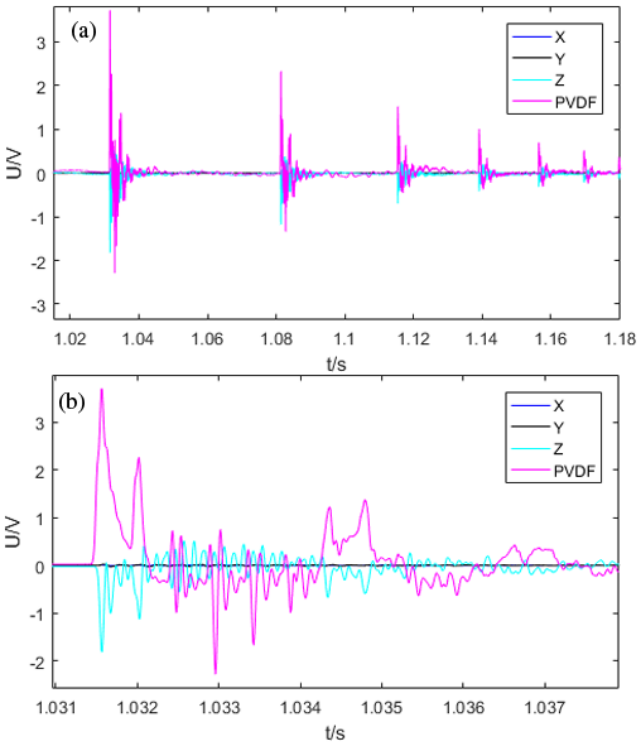


**Figure 9.** The output signal of the PVDF film and dynamometer. (a) The whole impact process; (b) one impact of the process. *X*, *Y* and *Z* represent the force in *x*, *y* and *z* direction of the dynamometer; PVDF represents the output charge of the PVDF film.

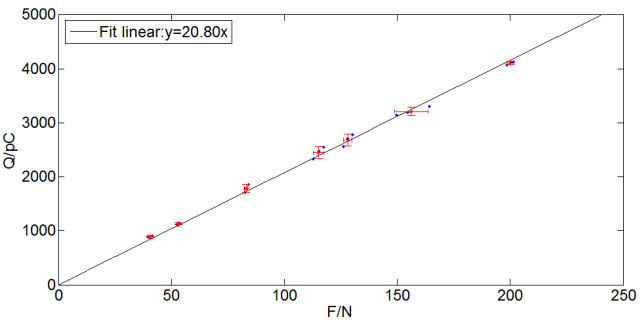


**Figure 10.** Fitting diagram of piezoelectric constant $d_{33}$ and the error bar of the measurement.

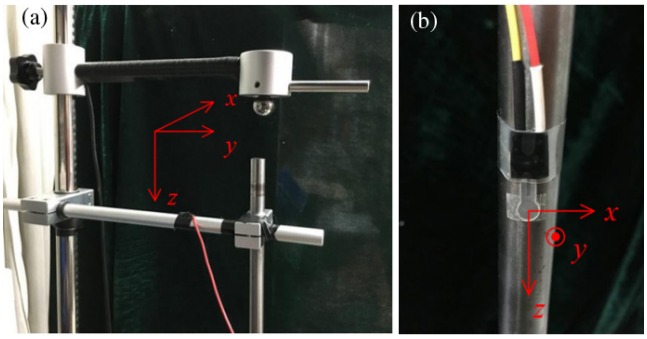


**Figure 11.** (a) The falling ball machine; (b) diagram of PVDF attached on the rod.

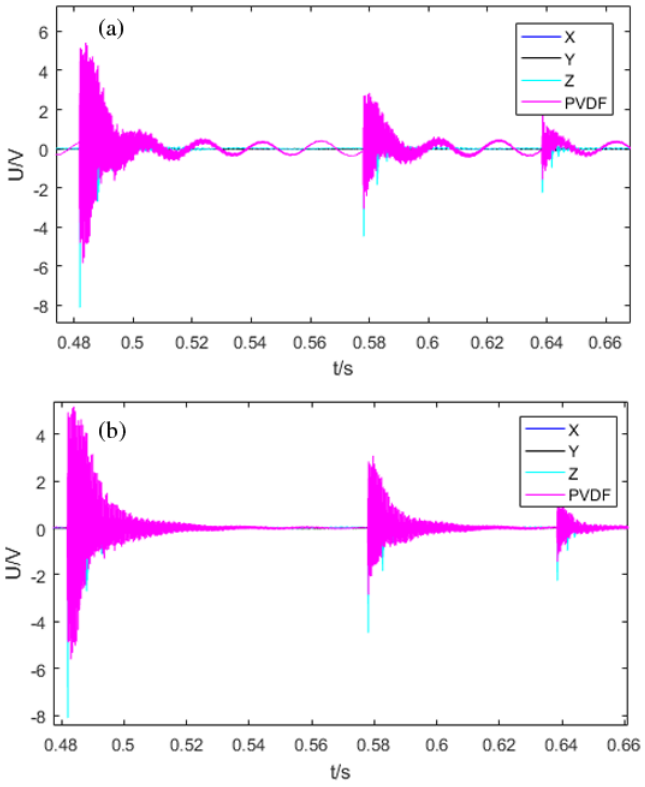


**Figure 12.** (a) The output results of PVDF and dynamometer; (b) the filtered result.

them is amplified as figure 9(b) shows. When the steel ball hits the thin rod and generates an impact, the impact will propagate vertically downward along the rod in the form of a mechanical wave. The mechanical wave will propagate first to the PVDF and then to the force platform. The experimental results in figure 9(b) also demonstrate that the time of the first peak of PVDF occurs earlier than the first peak of the piezoelectric force platform. After that, the mechanical wave will reflect and the reflected wave will propagate in the opposite direction to the incident wave. The reflected wave and the incident wave will be superimposed together. When the reflected wave reaches the top of the rod, it will continue to reflect (before the energy is attenuated) and superimpose. So there will be a lot of ripples after the first peak. Subsequent reflection and superimposition are complex processes and it is not very easy

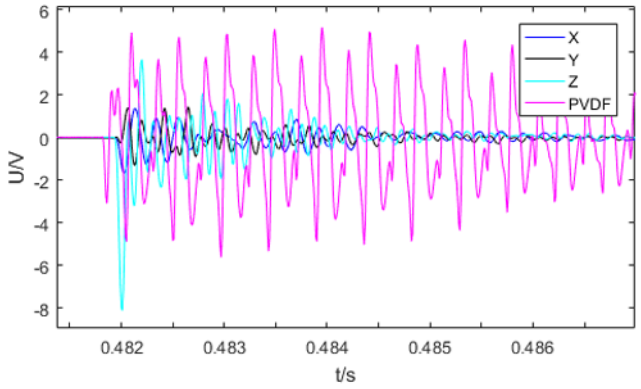


**Figure 13.** Amplification of impact signal.

to evaluate data. But the peak reached for the first time (possibly not the largest) is the result of only the impact and is not influenced by the superposition of reflected waves. We take the first peak value of the PVDF film and $Z$ force as the measurement results. The experiment was repeated and the measurement results are shown in table 3.

According to the experimental results, a scatter plot of the output charge and pressure and the error bar of the measurements are made as shown in figure 10. The value $d_{33} = 20.80$ pC N$^{-1}$ is obtained by fitting the curve with equation (6).

### *4.3. Calibration of piezoelectric constant in tensile mode*

As shown in figure 11(a), a steel ball with a mass of 55 g is selected to conduct the experiment. The effective area of the PVDF film is a 5 mm diameter circle, with PVDF film in the intermediate position of the rod attached by double-sided tape as shown in figure 11(b). Then we complete the dynamic calibration of the piezoelectric constant under the impact.

The measured results are shown in figure 12(a). The frequency of the electric supply is 50 Hz, and it will radiate in the form of electromagnetic waves. The PVDF film was interfered by this signal and there was a noise with a frequency of 50 Hz. Therefore, in the process of data processing, the first step was to filter the output signal of the PVDF film, writing a high-pass Butterworth filter in MATLAB software with a cut-off frequency set to 1000 Hz. The filtered result is shown in figure 12(b). In figure 12(b), it can be found that a falling ball can produce an impact more than once, and there is charge outputting at about 0.48 s, 0.58 s and 0.64 s. This is because after the steel ball fell on the press rod, it bounced up and fell down on the press rod. Only the signal generated on the process of the first fall is selected and amplified. As shown in figure 13, the impact time of the steel ball is only 0.07 ms. The relationship between the time of the impact and frequency is shown in equation (9) [24]:

$$f_r \tau = 0.78\sqrt{err_{\lim}} \tag{9}$$

where $\tau$ is the time of the impact, $f_r$ is the frequency that is represented by the impact and $err_{\lim}$ is the error limit. When the error limit is 5%, the impact lasting 0.07 ms represents a frequency of calibration of about 2.5 kHz. The piezoelectric

**Table 4.** Calibration data of $K$.

| $h$ (cm) | $\mu\varepsilon$ | $Q$ (pC) | $h$ (cm) | $\mu\varepsilon$ | $Q$ (pC) |
|---|---|---|---|---|---|
| 3 | 6.99 | 11.40 | 7 | 25.13 | 41.56 |
| 3 | 7.36 | 10.43 | 7 | 25.18 | 39.37 |
| 3 | 7.81 | 11.98 | 7 | 27.16 | 43.84 |
| 4 | 15.37 | 24.53 | 8 | 28.14 | 43.95 |
| 4 | 15.82 | 24.53 | 8 | 29.46 | 46.29 |
| 4 | 15.84 | 24.70 | 8 | 29.75 | 47.48 |
| 5 | 17.40 | 28.12 | 9 | 31.32 | 48.34 |
| 5 | 17.44 | 29.16 | 9 | 32.50 | 51.7 |
| 5 | 18.28 | 28.24 | 9 | 35.37 | 58.1 |
| 6 | 22.53 | 35.95 | 10 | 37.61 | 62.35 |
| 6 | 22.87 | 36.69 | 10 | 37.68 | 60.91 |
| 6 | 23.25 | 36.75 | 10 | 39.10 | 62.13 |

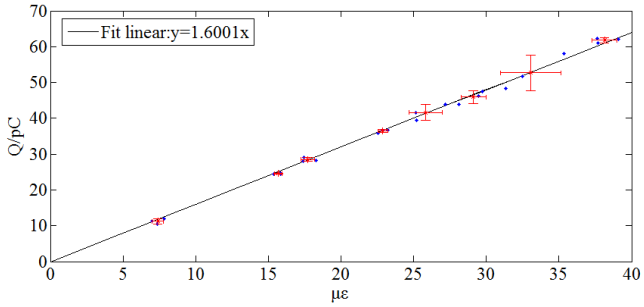


**Figure 14.** Strain–charge scatter diagram and fitting curve.

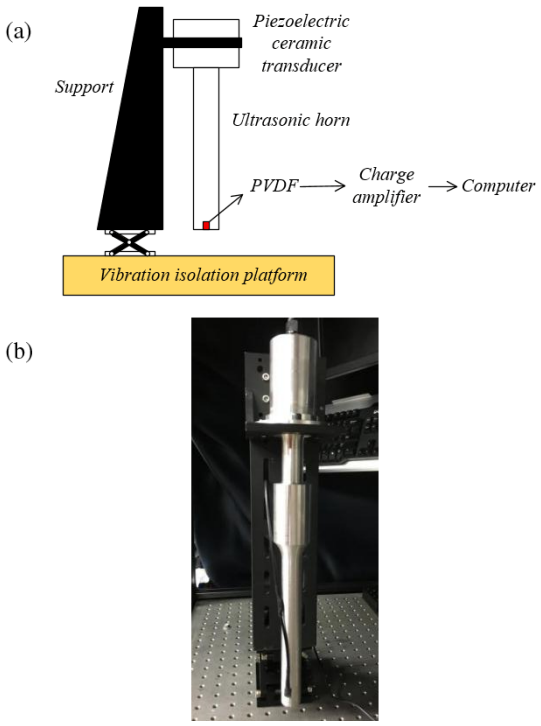


**Figure 15.** PVDF film measuring the strain of the horn. (a) Schematic diagram; (b) objects.

constant at 2.5kHz is not much different from that at ultrasonic frequency. So the piezoelectric constant at 2.5 kHz can represent the performance of PVDF at ultrasonic frequency.

Taking the first peak value of the PVDF film as its output value, there were still subsequent large peaks because of the

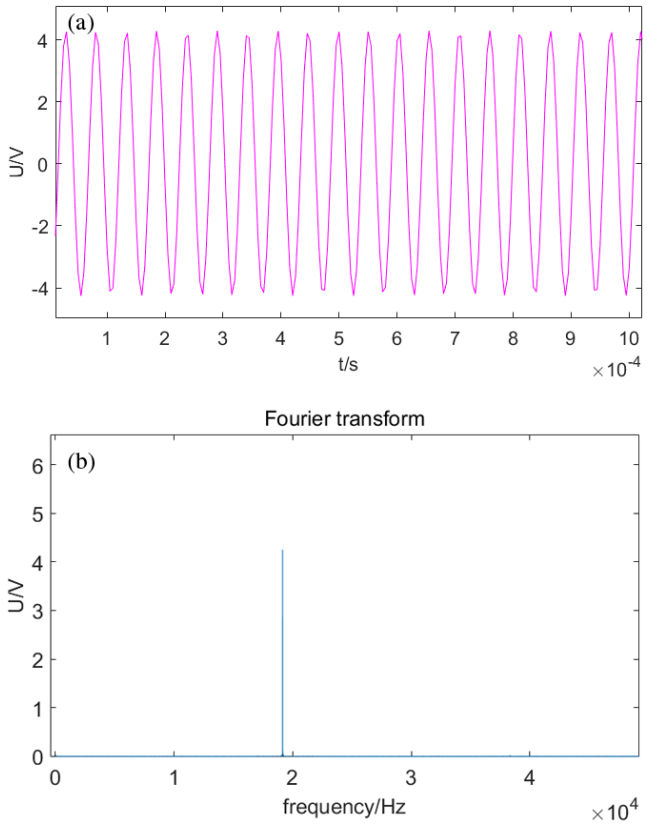


**Figure 16.** The result of peak-to-peak value is 80 V. (a) Measured signal; (b) Fourier transform signal.

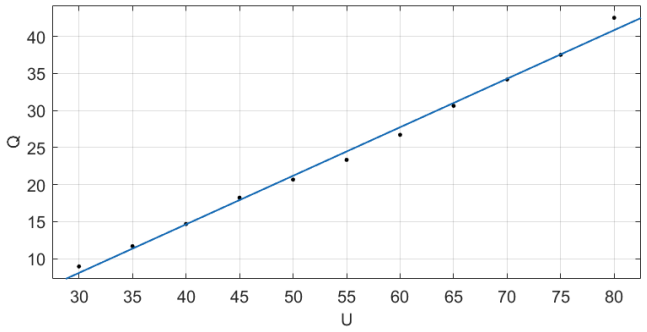


**Figure 17.** The relationship between the output charge of PVDF and the voltage of the transducer.

superposition of mechanical reflection waves in the thin rod. It can be observed from figure 13 that the first peak time of the PVDF film was earlier than that of the dynamometer, because the mechanical wave propagating from top to bottom firstly passed through the PVDF film and then acted on the platform. An impact signal has a short action time, so the frequency produced is relatively high and dynamic calibration is realized. We adjusted the drop height of the steel ball to generate different impact forces and repeated the experiment. The results are shown in table 4.

According to equation (7), the experimental data are calculated to obtain the strain caused by the rod, and the connection between the output charge of the PVDF film and strain is made. The slope of the strain–charge curve represents the responsivity of the PVDF film. As shown in figure 14, the

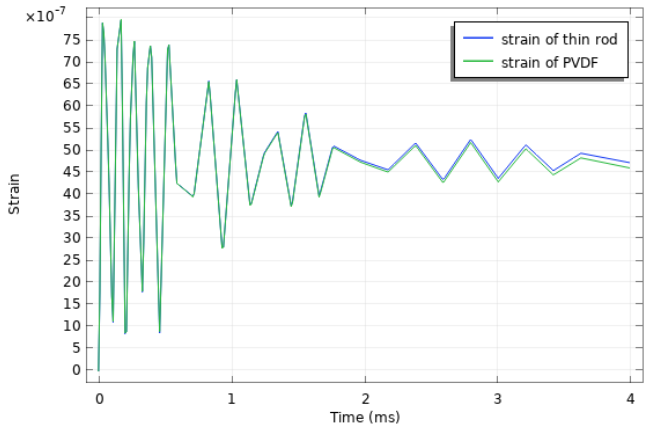


**Figure 18.** The strain of PVDF film and the thin rod.

fitting result is $K = 1.600\ \mathrm{pC}/\mu\varepsilon$ and the error bar of the measurement is also shown in figure 14.

### 4.4. Measurement of strain of ultrasonic horn

As shown in figure 15(a), the transducer and the horn were mounted on the bracket, and the PVDF film was pasted on the end of the transformer with double-sided tape to induce the strain at the end of the horn. The power supply of the transducer was a sinusoidal voltage with adjustable peak-to-peak value. The resonance frequency of the system was 19.157 kHz. The amplification factor of the charge amplifier of the PVDF film was 100 times. The signal acquisition frequency was 200 kHz and the acquisition time was 1 s. The measurement results are shown in figure 16. Fourier transform was performed on the measured results to obtain an output voltage of the PVDF film of 19.157 kHz. In the ultrasonic assisted vibration cutting experiment, the power supply voltage connected to the transducer could not be too low. Therefore, the power supply voltage was changed to be under the allowable conditions of the experiment. The results of voltage and output charge are shown in figure 17 when the paste position remained unchanged. It can be seen from figure 17 that the higher the voltage connected to the transducer, the larger the strain of the horn.

## 5. Uncertainty analysis

### 5.1. Analysis of systematic errors

*5.1.1. Environment.* In the experiment, the temperature of the laboratory is guaranteed to be constant at 26°. In order to eliminate electromagnetic interference, the connection line of PVDF is electromagnetically shielded.

*5.1.2. Position of the ball impact.* According to Saint Venant's principle, even if the impact position of the steel ball changes, it will not affect the strain distribution in the middle part of the rod.

**Table 5.** Repeated experiments of $d_{33}$ calibration.

| $Fz$/N | $Q$/pC | $Fz$/N | $Q$/pC | $Fz$/N | $Q$/pC |
|---|---|---|---|---|---|
| 196.9 | 4067 | 205.1 | 4184 | 204.5 | 4119 |
| 197.2 | 4077 | 198.7 | 4185 | 205.5 | 4120 |
| 193.9 | 4089 | 195.2 | 4185 | 204.0 | 4126 |
| 199.5 | 4092 | 203.1 | 4190 | 205.5 | 4134 |
| 203.4 | 4151 | 204.2 | 4153 | 196.9 | 4067 |
| 204.4 | 4153 | 203.8 | 4157 | 197.2 | 4077 |
| 193.9 | 4089 | 199.5 | 4092 | | |

*5.1.3. Tilt of the thin rod.* In the upper part of the thin rod, we placed a cylindrical sleeve to ensure that the thin rod is always placed vertically.

*5.1.4. Effect of double-sided tape.* In the calibration experiments for $d_{31}$, the PVDF film is attached to the thin rod with double-sided tape. In order to explore the effect of double-sided tape on PVDF film, a simulation model has been established by Comsol. We set the PVDF film and rod materials according to actual conditions and the material of the double-sided tape is set as a viscoelastic material. According to the experimental results, the impact force is applied to the rod. The simulation model analyzed the strain of the system. The strain curve over time on the PVDF film and the surface of the rod at the same height are shown in figure 18. It can be seen from figure 18 that the strain on the PVDF film and the rod is almost the same, so the influence of the double-sided tape can be ignored.

### 5.2. Uncertainty in $d_{33}$ calibration

In the whole experiment, the uncertainty of $d_{33}$ mainly comes from the uncertainty of the measured data during the experiment and the uncertainty of the fitting method, which are independent of each other. Therefore, the relative uncertainty of $d_{33}$ can be expressed by equation (10)

$$u_{\mathrm{rel}}^2(d_{33}) = u_{l,\mathrm{rel}}^2(d_{33}) + u_{m,\mathrm{rel}}^2(d_{33}), \tag{10}$$

where $u_{l,\mathrm{rel}}(d_{33})$ is the relative uncertainty caused by the nonlinearity of the fitting method, and $u_{m,\mathrm{rel}}(d_{33})$ is the relative uncertainty caused by the experimental measurement process.

*5.2.1. Relative uncertainty of the fitting method in $d_{33}$ calibration.* In this paper, the calibration of $d_{33} = 20.80\ \mathrm{pC\,N^{-1}}$ is the result of fitting with the least squares method based on multiple sets of experimental data. Statistical analysis is used to evaluate the relative uncertainty of the fitting method caused by nonlinear error. The uncertainty of the fitting method can be represented by the standard deviation of $d_{33}$.

$$u_l(d_{33}) = s\,(d_{33}) = 0.22\ \mathrm{pC\,N^{-1}}. \tag{11}$$

The relative uncertainty of the fitting method is $u_{l,\mathrm{rel}}\,(d_{33}) = \frac{u_l(d_{33})}{d_{33}} = 1.06\%$.

**Table 6.** Repeated experiments of $K$ calibration.

| $\mu\varepsilon$ | $Q_K$/PC | $\mu\varepsilon$ | $Q_K$/PC | $\mu\varepsilon$ | $Q_K$/PC |
|---|---|---|---|---|---|
| 19.13 | 31.83 | 19.30 | 32.15 | 19.50 | 31.70 |
| 19.17 | 31.60 | 19.36 | 32.25 | 19.56 | 32.84 |
| 19.26 | 34.19 | 19.41 | 30.90 | 19.77 | 31.81 |
| 19.23 | 31.84 | 19.50 | 34.58 | 19.82 | 34.26 |
| 19.94 | 30.75 | 20.57 | 32.25 | 20.42 | 31.65 |
| 19.98 | 34.47 | 20.61 | 33.10 | 20.51 | 33.35 |
| 20.66 | 31.41 | 20.80 | 30.54 | | |

*5.2.2. Relative uncertainty of the measured data in $d_{33}$ calibration.* The uncertainty of $d_{33}$ in the measurement process depends on the uncertainty of the inputs. According to equation (6), the relative uncertainty of $d_{33}$ can be expressed by

$$u_{m,\mathrm{rel}}(d_{33}) = \sqrt{u_{\mathrm{rel}}^2(Q) + u_{\mathrm{rel}}^2(F)}, \tag{12}$$

where $u_{m,\mathrm{rel}}(d_{33})$ is the relative uncertainty of $d_{33}$, $u_{\mathrm{rel}}(Q)$ is the relative uncertainty of charge, and $u_{\mathrm{rel}}(F)$ is the relative uncertainty of force.

The uncertainty of random error is analyzed by repeating the experiments under the same conditions. A steel ball of 55 g was selected to fall from the machine and the falling height was about 1.5 cm. Twenty experiments were carried out and the measured results are shown in table 5.

*5.2.2.1.Relative uncertainty of $Q$ in $d_{33}$ calibration.* In the repeated experiments shown in 5.1.2, the average charge is $\overline{Q} = 4139.9\,\mathrm{pC}$. The relative uncertainty of charge measurement consists of three parts:

$$u_{\mathrm{rel}}(Q) = \sqrt{u_{1,\mathrm{rel}}^2(Q) + u_{2,\mathrm{rel}}^2(Q) + u_{3,\mathrm{rel}}^2(Q)}, \tag{13}$$

where $u_{\mathrm{rel}}(Q)$ is the relative uncertainty of the charge, $u_{1,\mathrm{rel}}(Q)$ is the relative uncertainty of the repeated experiments, $u_{2,\mathrm{rel}}(Q)$ is the relative uncertainty of the charge amplifier, and $u_{3,\mathrm{rel}}(Q)$ is the relative uncertainty of reading.

The uncertainty of repeated experiments evaluated by the Bessel method is $u_1(Q) = \sqrt{\frac{\sum_{i=1}^{20}(Q_i-\overline{Q})^2}{20(20-1)}} = 8.66\,\mathrm{pC}$. The relative uncertainty of repeated experiments is $u_{1,\mathrm{rel}}(Q) = \frac{u_1(Q)}{\overline{Q}} = 0.21\%$.

The extended uncertainty of the charge amplifier is $U_{95} = 1.0\%$ and the relative uncertainty is $u_{2,\mathrm{rel}}(Q) = \frac{U_{95}}{2} = 0.50\%$ estimated by normal distribution.

In this experimental condition, the division value of the charge amplifier is 1 pC. Then the relative uncertainty is $u_{3,\mathrm{rel}}(Q) = \frac{0.5}{\overline{Q}} = 0.01\%$.

Therefore, according to the equation (13), the relative uncertainty of charge is $u_{\mathrm{rel}}(Q) = 0.54\%$.

*5.2.2.2.Relative uncertainty of $F$ in $d_{33}$ calibration.* In the repeated experiments shown in 5.1.2, the average of force is $\overline{F} = 201.7N$. The uncertainty of force measurement consists of three parts:

$$u_{\mathrm{rel}}(F) = \sqrt{u_{1,\mathrm{rel}}^2(F) + u_{2,\mathrm{rel}}^2(F) + u_{3,\mathrm{rel}}^2(F)}, \tag{14}$$

where $u_{\mathrm{rel}}(F)$ is the relative uncertainty of the force, $u_{1,\mathrm{rel}}(F)$ is the relative uncertainty of the repeated experiments, $u_{2,\mathrm{rel}}(F)$ is the relative uncertainty of the dynamometer, and $u_{3,\mathrm{rel}}(F)$ is the relative uncertainty of reading.

The uncertainty of repeated experiments evaluated by the Bessel method is $u_1(F) = \sqrt{\frac{\sum_{i=1}^{20}(F_i-\overline{F})^2}{20(20-1)}} = 0.92\mathrm{N}$. The relative uncertainty of repeated experiments is $u_{1,\mathrm{rel}}(F) = \frac{u_1(F)}{\overline{F}} = 0.45\%$.

The extended uncertainty of the dynamometer is $U_{95} = 0.19\%$ and the relative uncertainty is $u_{2,\mathrm{rel}}(F) = \frac{U_{95}}{2} = 0.095\%$ estimated by normal distribution.

In this experimental condition, the division value of the charge amplifier is 0.1 N. Then the relative uncertainty is $u_{3,\mathrm{rel}}(F) = \frac{0.05}{\overline{F}} = 0.02\%$.

Therefore, according to equation (14), the relative uncertainty of force is $u_{\mathrm{rel}}(F) = 0.46\%$. Finally, the relative uncertainty of $d_{33}$ produced by the measurement is $u_{m,\mathrm{rel}}(d_{33}) = \sqrt{u_{\mathrm{rel}}^2(Q) + u_{\mathrm{rel}}^2(F)} = 0.71\%$.

According to equation (10), the relative uncertainty of the calibration result is $u_{\mathrm{rel}}(d_{33}) = 1.28\%$.

### 5.3. Uncertainty in K calibration

In the experiment, the uncertainty of $K$ mainly comes from the uncertainty of the measured data during the experiment and the uncertainty of the fitting method, which are independent of each other. Therefore, the relative uncertainty of $K$ can be expressed by equation (15)

$$u_{\mathrm{rel}}^2(K) = u_{l,\mathrm{rel}}^2(K) + u_{m,\mathrm{rel}}^2(K), \tag{15}$$

where $u_{\mathrm{rel}}(K)$ is the relative uncertainty of $K$, $u_{l,\mathrm{rel}}(K)$ is the relative uncertainty caused by the nonlinearity of the fitting method, and $u_{m,\mathrm{rel}}(K)$ is the relative uncertainty caused by the experimental measurement process.

*5.3.1. Relative uncertainty of the fitting method in $K$ calibration.* Similar to 5.1.1, we can get $K = 1.600\,\mathrm{pC}/\mu\varepsilon$ and the uncertainty of the fitting method in $K$ calibration is $u_l(K) = s(K) = 0.024\,\mathrm{pC}/\mu\varepsilon$. The relative uncertainty is $u_{l,\mathrm{rel}}(K) = \frac{u_l(K)}{K} = 1.48\%$.

*5.3.2. Relative uncertainty of the measured data in $K$ calibration.* The uncertainty of $K$ in the measurement process depends on the uncertainty of the inputs. According to the equation (8), the relative uncertainty of $K$ can be expressed by equation (16):

$$u_{m,\mathrm{rel}}(K) = \sqrt{u_{\mathrm{rel}}^2(Q_K) + u_{\mathrm{rel}}^2(\varepsilon)}. \tag{16}$$

where $u_{m,\mathrm{rel}}(K)$ is the relative uncertainty of $K$, $u_{\mathrm{rel}}(Q_K)$ is the relative uncertainty of charge, and $u_{\mathrm{rel}}(\varepsilon)$ is the relative uncertainty of the strain.

The uncertainty of random error is analyzed by repeating experiments under the same conditions. A steel ball of 55 g was selected to fall from the machine and the falling height

was about 8 cm. Twenty experiments were carried out and the measured results are shown in table 6.

*5.3.2.1.Relative uncertainty of $Q_K$ in $K$ calibration.* In the repeated experiments shown in 5.2.2, the average charge $\overline{Q_K} = 32.37\,\text{pC}$. The uncertainty of charge measurement consists of three parts and can be expressed by equation (17):

$$u_{\text{rel}}(Q_K) = \sqrt{u_{1,\text{rel}}^2(Q_K) + u_{2,\text{rel}}^2(Q_K) + u_{3,\text{rel}}^2(Q_K)}, \quad (17)$$

where $u_{\text{rel}}(Q_K)$ is the relative uncertainty of the charge, $u_{1,\text{rel}}(Q_K)$ is the relative uncertainty of the repeated experiments, $u_{2,\text{rel}}(Q_K)$ is the relative uncertainty of the charge amplifier, and $u_{3,\text{rel}}(Q_K)$ is the relative uncertainty of reading.

The uncertainty of repeated experiments evaluated by the Bessel method is $u_1(Q_K) = \sqrt{\frac{\sum_{i=1}^{20}(Q_{Ki}-\overline{Q_K})^2}{20(20-1)}} = 0.28\,\text{pC}$. The relative uncertainty of repeated experiments is $u_{1,\text{rel}}(Q_K) = \frac{u_1(Q_K)}{\overline{Q_K}} = 0.856\%$.

The extended uncertainty of the charge amplifier is $U_{95} = 1.0\%$ and the relative uncertainty is $u_{2,\text{rel}}(Q_K) = \frac{U_{95}}{2} = 0.50\%$ estimated by normal distribution.

In this experimental condition, the division value of the charge amplifier is 0.01 pC. Then the relative uncertainty is $u_{3,\text{rel}}(Q_K) = \frac{0.005}{\overline{Q_K}} = 0.015\%$.

Therefore, according to equation (17), the relative uncertainty of charge is $u_{\text{rel}}(Q_K) = 0.991\%$.

*5.3.2.2.Relative uncertainty of strain in $K$ calibration.* According to equation (7), the Young's modulus of the rod and Pi are regarded as constants and the uncertainty of strain measurement consists of two parts:

$$u_{\text{rel}}^2(\mu\varepsilon) = u_{\text{rel}}^2(F_K) + 4u_{\text{rel}}^2(d), \quad (18)$$

where $u_{\text{rel}}(\mu\varepsilon)$ is the relative uncertainty of the strain, $u_{\text{rel}}(F_K)$ is the relative uncertainty of the force, and $u_{\text{rel}}(d)$ is the relative uncertainty of the diameter of the rod.

In the repeated experiments shown in 5.2.2, the average force is $\overline{F_K} = 829.1N$. The uncertainty of the force measurement consists of three parts:

$$u_{\text{rel}}(F_K) = \sqrt{u_{1,\text{rel}}^2(F_K) + u_{2,\text{rel}}^2(F_K) + u_{3,\text{rel}}^2(F_K)}, \quad (19)$$

where $u_{1,\text{rel}}(F_K)$ is the relative uncertainty of the repeated experiments, $u_{2,\text{rel}}(F_K)$ is the relative uncertainty of the dynamometer, and $u_{3,\text{rel}}(F_K)$ is the relative uncertainty of reading.

The uncertainty of repeated experiments evaluated by the Bessel method is $u_1(F_K) = \sqrt{\frac{\sum_{i=1}^{20}(F_{Ki}-\overline{F_K})^2}{20(20-1)}} = 5.291N$. The relative uncertainty of repeated experiments is $u_{1,\text{rel}}(F_K) = \frac{u_1(F_K)}{\overline{F_K}} = 0.638\%$.

The extended uncertainty of the dynamometer is $U_{95} = 0.19\%$ and the relative uncertainty is $u_{2,\text{rel}}(F_K) = \frac{U_{95}}{2} = 0.095\%$ estimated by normal distribution.

In this experimental condition, the division value of the charge amplifier is 0.1 N. Then the relative uncertainty is $u_{3,\text{rel}}(F_K) = \frac{0.05}{\overline{F_K}} = 0.006\%$.

Therefore, according to equation (19), the relative uncertainty of force is $u_{\text{rel}}(F_K) = 0.645\%$.

The nominal diameter of the rod is $d = 16\,\text{mm}$. The uncertainty of the diameter consists of two parts:

$$u(d) = \sqrt{u_1^2(d) + u_2^2(d)}, \quad (20)$$

where $u(d)$ is the uncertainty of the diameter, $u_1(d)$ is the uncertainty of the indication of the micrometer, and $u_2(d)$ is the uncertainty of operation of the user.

The maximum allowable error of the micrometer is $\pm 3\,\mu\text{m}$ and the uncertainty is $u_1(d) = \frac{3\,\mu\text{m}}{\sqrt{3}} = 1.73\,\mu\text{m}$ estimated by rectangular distribution.

According to the experiments, the measurement error produced by the user is $\pm 10\,\mu\text{m}$ and the uncertainty is $u_2(d) = \frac{10\,\mu\text{m}}{\sqrt{3}} = 5.77\,\mu\text{m}$ estimated by rectangular distribution.

It is known from equation (20) that the uncertainty of the diameter is $u(d) = 6.02\,\mu\text{m}$ and the relative uncertainty of the diameter is $u_{\text{rel}}(d) = 6.02 \times 10^{-3} \div 16 = 0.038\%$.

The relative uncertainty of the strain is $u_{\text{rel}}(\mu\varepsilon) = 0.649\%$ and the relative uncertainty of $K$ produced by the measurement is $u_{m,\text{rel}}(K) = \sqrt{u_{\text{rel}}^2(Q_K) + u_{\text{rel}}^2(\mu\varepsilon)} = 1.185\%$. According to equation (15), the relative uncertainty of the calibration result is $u_{\text{rel}}(K) = 1.896\%$.

## 6. Conclusions

In this paper, the impact force generated by the falling steel ball acts on the thin rod and the uneven stress produces uniform strain on the thin rod over 40 cm above the working point.

The piezoelectric constant in the tension direction of the PVDF film was calibrated using this property. For the PVDF film selected in the experiment, the responsivity on the tension direction was 1.600 pC/$\mu\varepsilon$, and the relative uncertainty of the measurement was 1.896%; the piezoelectric constant in the thickness direction was 20.80 pC $\text{N}^{-1}$, and the relative uncertainty of the measurement was 1.28%. Compared with the traditional calibration method, the impact signal action time was shorter, at about 0.07 ms. Moreover, the dynamic response was better, and was closer to the working state under ultrasonic frequency.

We conduct the strain measurements with well-calibrated piezoelectric thin film, taking the ultrasonic transducer and the horn as examples to verify the correctness of the calibration of the piezoelectric constant. Choosing the horn with a resonant frequency of 19.157 kHz, it could be found that the strain generated at the end of the horn was 21.6 $\mu\varepsilon$ when the peak-to-peak amplitude value of the sine signal was 80 V. It was proven in this paper that the calibration method was applicable to measurement under ultrasonic frequency.

## Funding

This research was funded by Tianjin Natural Science Foundation, Grant Nos. 17JCYBJC19000 and 18JCZDJC31800.

## ORCID iDs

Yelong Zheng https://orcid.org/0000-0002-8204-946X

## References


[1] Kubota M, Kanno T and Murata Y 2017 The efficacy of a released ultrasonic lithotripsy in percutaneous nephrolithotomy: randomized trial comparing Swiss LithoClast® Master versus Swiss LithoClast® *Hinyokika kiyo. Acta Urologica Japonica.* **63** 1–5

[2] Verhaagen B, Zanderink T and Rivas D F 2016 Ultrasonic cleaning of 3D printed objects and cleaning challenge devices *Appl. Acoust.* **103** 172–81

[3] Feng Z, Zhou X and Xu S 2018 Impacts of humidification process on indoor thermal comfort and air quality using portable ultrasonic humidifier *Build. Environ.* **133** 62–72

[4] Zhou G, Xu G and Liu J 2018 Assessment of laser weld width based on time and frequency domains of ultrasonic testing signals *J. Mater. Process. Technol.* **251** 175–80

[5] Chu N H, Nguyen D B and Ngo N K 2018 A new approach to modelling the drilling torque in conventional and ultrasonic assisted deep-hole drilling processes *Appl. Sci.* **8** 2600

[6] Chu N H and Nguyen V D 2018 Ultrasonic-assisted cutting: a beneficial application for temperature torque reduction and cutting ability improvement in deep drilling of Al-6061 *Appl. Sci.* **8** 1708

[7] Totis G and Sortino M 2011 Development of a modular dynamometer for triaxial cutting force measurement in turning *Int. J. Mach. Tools Manuf.* **51** 34–42

[8] Kim D and Jeon D 2011 Fuzzy-logic control of cutting forces in CNC milling processes using motor currents as indirect force sensors *Precis. Eng.* **35** 143–52

[9] Petrović P B, Pavlović V B and Vlahović B 2018 A high-sensitive current-mode pressure/force detector based on piezoelectric polymer PVDF *Sens. Actuators* A *Physical.* **276** 165–75

[10] Lee J S, Shin K Y and Cheong O J 2015 Highly sensitive and multifunctional tactile sensor using free-standing ZnO/PVDF thin film with graphene electrodes for pressure and temperature monitoring *Sci. Rep.* **5** 7887

[11] Bae J H and Chang S H 2019 PVDF-based ferroelectric polymers and dielectric elastomers for sensor and actuator applications: a review *Funct. Compos. Struct.* **1** 012003

[12] Persano L, Dagdeviren C and Su Y 2013 High performance piezoelectric devices based on aligned arrays of nanofibers of poly *Nat. Commun.* **4** 1633

[13] Hu Y, Kang W and Fang Y 2018 Piezoelectric poly (vinylidene fluoride)(PVDF) polymer-based sensor for wrist motion signal detection *Appl. Sci.* **8** 836

[14] Xin Y, Sun H and Tian H 2016 The use of polyvinylidene fluoride (PVDF) films as sensors for vibration measurement: a brief review *Ferroelectrics* **502** 28–42

[15] AlMohimeed I, Agarwal M and Ono Y 2018 Wearable ultrasonic sensor using double-layer PVDF films for monitoring tissue motion (IEEE CCECE) pp 1–4

[16] Wang Y Q and Xiao Y L 2014 A dynamic calibration test on PVDF film pressure sensor with dropping hammer method *Adv. Mater. Res.* **933** 548–53

[17] Ni N, Wang Y and Liu F 2014 A new dielectric elastomer sensor based on cantilever beam structure with constant strength *Appl. Mech. Mater.* **664** 279–83

[18] Stewart M and Cain M G 2014 Direct piezoelectric measurement: the Berlincourt method *Characterisation of Ferroelectric Bulk Materials and Thin Films* (Dordrecht: Springer) pp 37–64

[19] Liu J M *et al* 2002 Piezoelectric coefficient measurement of piezoelectric thin films: an overview *Mater. Chem. Phys.* **75** 12–8

[20] Van Nuffel D, Peirs J and De Baere I 2012 Calibration of dynamic piezoelectric force transducers using the Hopkinson bar technique *15th International Conference on Experimental Mechanics (Porto, Portugal, 22–27 July 2012)* ed J F Silva Gomes and M A P Vaz (Porto: INEGI) 3068 pp 1–12

[21] Wei X, Yang Y and Yao W 2017 PSpice modeling of a sandwich piezoelectric ceramic ultrasonic transducer in longitudinal vibration *Sensors* **17** 2253

[22] Ling M, Cao J, Li Q and Zhuang J 2018 Design, pseudostatic model, and PVDF-based motion sensing of a piezo-actuated *XYZ* flexure manipulator *IEEE/ASME Trans. Mechatronics* **23** 2837–48

[23] Ma X J and Wang L L 2005 Research on the dynamic calibration of PVDF Gauges loaded with lower stresses *J. Ningbo Univ. (Nat. Sci. Eng.)* **4** 435–8

[24] Deheng P, Hongian L and Shuguang W 1988 An automatic dynamic response calibration system for high-pressure transducers *IEEE Instrumentation & Measurement Technology Conf.* 43–6